84% Catalyst Activity of Water-Assisted Growth of Single Walled Carbon Nanotube Forest Characterization by a Statistical and Macroscopic Approach

Don N. Futaba, Kenji Hata,* Tatsunori Namai, Takeo Yamada, Kohei Mizuno, Yuhei Hayamizu, Motoo Yumura, and Sumio Iijima

Research Center for Advanced Carbon Materials, National Institute of Advanced Industrial Science and Technology (AIST), Tsukuba, 305-8565, Japan, and Japan Fine Ceramics Center, National Institute of Advanced Industrial Science and Technology (AIST), Tsukuba, 305-8565, Japan

Received: January 5, 2006; In Final Form: February 23, 2006

We propose a statistical and macroscopic analysis to estimate the catalyst activity of water-assisted growth (super-growth) of single-walled nanotubes (SWNT) and to characterize SWNT forests. The catalyst activity was estimated to be 84% (±6%), the highest ever reported. The SWNT forest was found to be a very sparse material where SWNTs represent only 3.6% of the total volume. This structural sparseness is believed to play a critical role in achieving highly efficient growth.

Chemical vapor deposition (CVD) possesses promising characteristics, such as scalability and controllability, and has thus become the standard method for SWNT synthesis. However, CVD has suffered severely from low catalyst activity, i.e., only a few percent of the catalysts produce carbon nanotubes (CNT), while the majority of the catalysts remain inactive. The low catalytic activity of CNT synthesis has not only limited the availability of SWNTs, but the inactivated catalysts remain in the as-grown material as impurities and can constitute a significant fraction of the as-grown product, necessitating chemical purification for their removal.

A significant breakthrough addressing this low efficiency has been achieved by the addition of a small and controlled amount of water into a CVD growth (henceforth denoted as "Super-Growth CVD"),[1] which results in the massive growth of highly dense vertically aligned impurity-free SWNT forests with millimeter-scale heights on substrates with catalyst densities below one monolayer. SWNT forests[2] represent a new form of SWNT material and, as was done by its kin, MWNT forests, is envisioned to open new opportunities for scientific research and to enable the development of new and improved applications ranging from optical polarizers[3] to nanoporous membranes.[4]

While the speculated catalyst activity for super-growth CVD is high, the accurate estimation remains unknown. Therefore, characterization of SWNT forests is indispensable to unlock their full potential for both fundamental research and application development. With this in mind, we present here a new macroscopic and statistical approach to characterize important quantities, such as catalyst activity of super-growth, mass density, and tube density of SWNT forests in a reliable manner. Our approach is quite distinct from previous attempts at characterization in the sense that it is both macroscopic and statistical. Ishida et al.[5] performed a microscopic and statistical analysis by atomic force microscopy for their SWNTs grown from lithographically defined nanoparticles and reported a 10% catalyst activity, yet this approach is susceptible to overlooking variations on a large scale.

* Address correspondence to this author at the National Institute of Advanced Industrial Science and Technology. E-mail: kenji-hata@aist.go.jp.

The macroscopic and statistical analysis was carried out on a precisely cut (by dicing saw) 2 × 2 cm^2 Si substrate (600 nm oxidized layer), with a SWNT forest ∼1 mm in height with uniformity within a margin of ∼20 μm (Figure 1a, inset). A sequentially sputtered Al_2O_3 (10 nm) then Fe (1.2 nm) metal layer was deposited. The substrate was placed in a 1 in. diameter quartz tube furnace and upon annealing the Fe metal thin film converted into well-isolated individual catalyst nanoparticles,[6] and a SWNT forest was grown by super-growth CVD at 750 °C with an ethylene (99.999%) carbon source and water catalyst enhancer and preserver.[7] The water concentration was measured by a water-monitor directly connected to the exhaust line. Pure He (99.9999%) with 40% H_2 (99.99999%) (total flow 1000 cm^3 STP per minute) was used as a carrier gas at 1 atm with a small and controlled amount of water vapor supplied from the water bubbler. CVD growth was carried out with ethylene at 100 cm^3 STP per minute and water concentration of 150 ppm for 10 min as the standard growth time.[1] The CNTs were confirmed to be SWNTs through detailed analysis by transmission electron microscopy (TEM) and Raman spectroscopy as described in the following.

We found that our SWNT forests possess vertical mass uniformity. We plotted the weight of the SWNT forest for varying growth times as a function of height as shown in Figure 1a. To ensure maximum consistency, all of the samples were prepared by a single sputtering batch (which has shown only 5% spatial variation). The weight increased linearly with the height indicating vertical mass uniformity. For each height the forest mass density was calculated and plotted (dotted line in Figure 1a), and was constant at 0.037(±0.002) g/cm^3.[8] This is much lower than that of a SWNT (1.3 g/cm^3) or graphitic carbon (2.25 g/cm^3) indicating the sparseness of the SWNT forest.

It follows that any 2-D cross-section of the SWNT forest can be considered identical and affords us to directly compare a 2-D forest cross-section with the 2-D catalyst containing substrate (Figure 1b). The catalyst activity can then simply be calculated from

$$\eta = n(\mathrm{SWNT})/n(\mathrm{cat}) \qquad (1)$$

where η is the catalyst activity, n(SWNT) is the SWNT area

10.1021/jp060080e CCC: $30.25
Published on Web 03/25/2006

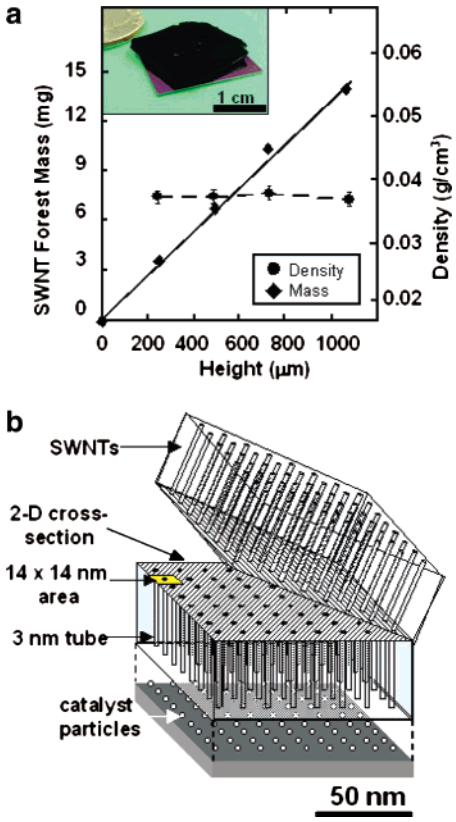

Figure 1. Forest uniform mass density. (a) Plot of the SWNT forest mass as a function of height (solid line). Circles represent the calculated density for each height (dashed line). Inset: Photograph of the macroscopically large SWNT forest sample (2 × 2 cm, ~1 mm tall) used for this analysis (after several TEM samples had been removed). (b) Schematic representation of the SWNT forest illustrating the uniformity of the SWNT forest, the 2-D cross-sectional surface, and the catalyst coated substrate surface.

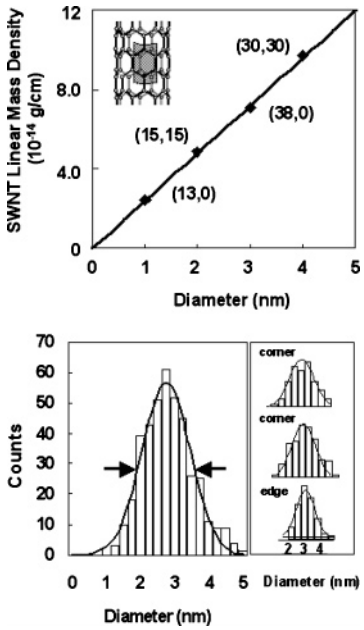

Figure 2. Linear mass density. (a) Plot of the calculated linear mass density for an individual SWNT as a function of diameter from an atomic model. The calculated linear mass density for two armchair and zigzag examples is marked with diamonds. The framework for the linear mass density was derived from the calculation of the mass of an individual SWNT. Because the mass is the product of its surface area and a surface mass density and the surface area is a product of the length and circumference, the linear mass density was found to be simply a linear function of the diameter. Therefore, from the atomic model (inset), a unit cell, which could be used as a basis for lattice vectors spanning the tube surface, provides a precise determination of the surface mass density. (b) SWNT diameter distribution histogram from TEM analysis of the center of the forest. Inset: Diameter distributions of different locations of the sample: corner, corner, and side, respectively.

density (cm^{-2}), and n(cat) is the catalyst area density (cm^{-2}). The SWNT area density can be deduced from the forest mass density as

$$\rho = n(\mathrm{SWNT}) \times \lambda(\mathrm{av}) \qquad (2)$$

where ρ is the forest mass density (g/cm^3), n(SWNT) is the SWNT area density (cm^{-2}), and λ(av) is the average linear mass density (g/cm) defined as the average mass of a SWNT per unit length. Equation 2 holds true because the super-growth as-grown product is almost totally SWNTs.[1] These equations form the basic foundation of our statistical and macroscopic analysis.

SWNTs with different diameters, predictably, have different linear mass densities. The linear mass density of a SWNT with arbitrary index (n,m) can be exactly obtained by considering its atomic model. From the unit cell of the atomic model, the surface mass density for an individual SWNT can be calculated from which the linear mass density can be deduced (Figure 2a). Interestingly, the linear mass density is simply a linear function of the diameter and is almost independent of the chirality. Despite the extreme chirality difference, armchair and zigzag SWNTs follow the overall trend for the linear mass densities (Figure 2a). Consequently, estimation of the average linear mass density of the forest requires the average SWNT diameter of the forest. While Raman spectroscopy can be macroscopic, and the radial breathing modes peaks (RBM) correspond to specific diameters of SWNTs, it is not adequate because an accurate and quantitative diameter distribution of SWNTs cannot be obtained.[9] The only manner to obtain an unambiguous quantitative distribution of diameters for SWNTs is to resort to microscopic methods, such as TEM. Diameters for 407 SWNT TEM images were measured, plotted in a histogram (Figure 2b), and a Gaussian distribution was fitted to locate the mean diameter, which was determined to be 3.0 nm with a standard deviation (SD) of 0.7 nm.

We proceeded to translate this microscopic evaluation into a macroscopic estimation. First, TEM diameter distribution evaluation (inset of Figure 2b) was repeated for several locations, such as the edge and two corners, to provide a reasonable sampling throughout our sample. The mean diameters were 2.9, 3.0, and 3.1 nm, respectively, showing good agreement with the mean diameter of the center. This strongly suggests that the forest possesses a very good homogeneity in terms of diameter distribution throughout the sample. Moreover, in total, 868 SWNTs were measured throughout the forest, and the overall mean diameter was 3.0 nm with a SD of 0.7 nm, showing excellent agreement with the value at the center of the forest. Calculation of the standard error on the mean yielded a value of 0.07 nm.[10] This represents an uncertainty in the mean of only 2.3%.

Additionally, Raman spectroscopy line mapping of the forest further supported vertical uniformity. After cleaving the forest along its midsection to reveal a cross-sectional surface, vertical and horizontal Raman line mappings at 532 nm showed exceptional uniformity (Figure 3). The relative intensities of the G-band and the D-band were quite constant throughout the mapping indicating uniform quality of the SWNTs inside the forest. More importantly, the intensities and locations of the

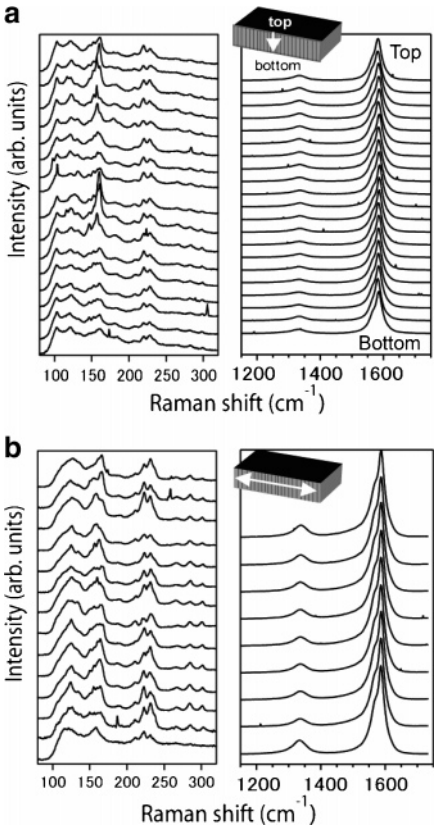

Figure 3. Raman line mapping. (a) Vertical Raman spectroscopy line mapping of the G-band to D-band from top to bottom. Inset: Vertical line mapping of the RBM spectra spanning the forest height. (b) Horizontal Raman line mapping of the G-band to D-band traversing the 2 cm midsection of the sample. Inset: Horizontal line mapping of the RBM spectra spanning the same 2 cm midsection.

RBM peaks were consistent throughout the mapping (within the reliability of our instrument) with characteristic RBM peaks observed at 125, 158, 211, 223, 231, 266, 284, and 301 cm^{-1}. The RBM frequency (cm^{-1}) is related to the SWNT diameter by the relation $\omega = 248/d$, where ω is the RBM frequency (cm^{-1}) and d is the diameter of SWNTs (nm).[11] The shortcoming of the RBM analysis is that SWNTs larger than 3 nm were unmeasurable because their corresponding RBM frequencies are too low for our instrument. However, the uniformity in RBM peaks in Raman mapping for an arbitrary cross-sectional face strongly supports a uniform SWNT diameter distribution throughout the forest. Combining the TEM and Raman results, we conclude that the forest SWNT diameter distribution is highly uniform, and thus we consider the size distribution obtained by TEM to represent the forest as a whole. It is interesting to note that the RBM peaks mapped in the vertical direction were essentially the same from the top to the bottom. This provides clear evidence that lateral growth is suppressed in super-growth on a millimeter scale and indicates that higher SWNT forests might be achievable in the future.

Combining the experimental results with eq 2 enables us to perform statistical and macroscopic characterization of the forest giving insight into the structure. First, existence probabilities for SWNTs possessing given diameters were calculated from the diameter distribution obtained by TEM observation. We then integrated the corresponding linear mass densities over the full diameter range to obtain a weighted average linear mass density: 7.1×10^{-14} g/cm ($\pm 2.3\%$).[12] Finally, from eq 2, the SWNT area density is $5.2 \times 10^{11}(\pm 0.35 \times 10^{11})$ tubes/cm^2. As summarized in Table 1, the mass density of the forest

TABLE 1: Summary of the Structural Characteristics of Super-Growth SWNT Forests

SWNT forest mass density	$0.037(\pm 0.002)$ g/cm^3
av diameter	$3.0(\pm 0.07)$ nm
SWNT area density	$5.2 \times 10^{11}(\pm 0.35 \times 10^{11})$ tubes/cm^2
coverage	3.6%
area per tube	14 nm × 14 nm
catalyst activity	$84(\pm 6)$%

is $0.037(\pm 0.002)$ g/cm^3, the average SWNT size is $3.0(\pm 0.07)$ nm, and the SWNT area density is $5.2 \times 10^{11}(\pm 0.35 \times 10^{11})$ tubes/cm^2. This means that on average there exists one 3 nm diameter SWNT in a substrate area of 190 nm^2 and the average distance between tubes is 14 nm. Consequently, the SWNTs occupy 3.6% of the total volume, thus meaning that more that 96% is empty space. A schematic of the forest assuming complete uniformity is given in Figure 1b for clarity.

We believe the sparseness of the forest is essential for growing SWNT forests by CVD where the catalysts remain on the substrate during growth (root growth) as is the case for super-growth. We suspect that excessively high densities inhibit carbon diffusion to the catalysts (diffusion limited), whereas, for insufficiently high densities, the SWNTs would fail to grow vertically and form a mat and likely quickly suffocate the catalysts as observed in normal CVD. We believe that the sparse condition is critical in achieving highly efficient SWNT growth on substrates, because only with this condition can vast amounts of SWNTs be grown on a substrate while not restricting the delivery of the carbon feedstock. The catalysts used in super-growth CVD were designed in structure to meet these criteria, and the growth conditions were tuned to optimize the height of forest growth. We expect a range of density conditions exist that is suitable to produce SWNT forests, thereby enabling highly efficient growth, and anticipate that the current work will stimulate further efforts to address this important issue.

With the SWNT area density estimated, the catalyst activity for super-growth can be determined from eq 1 provided the catalyst area density is known (Figure 1b). After physically or chemically (by oxygen plasma) removing the forest (which showed less than a 3% difference), we examined the catalyst substrate by microscopic methods. High-resolution scanning electron microscopy (SEM) served as the best method for this purpose. The contrast of secondary electron scattering of the iron catalyst nanoparticles and the surrounding alumina substrate was such that the individual Fe catalyst nanoparticles could be observed clearly (Figure 4: SEM image). We are confident that the observed particles are Fe because in control experiments with only an Al_2O_3 layer they were not observed. SEM images show well-separated and uniform individual Fe nanoparticles. We expect that particles about 1 nm or less would be

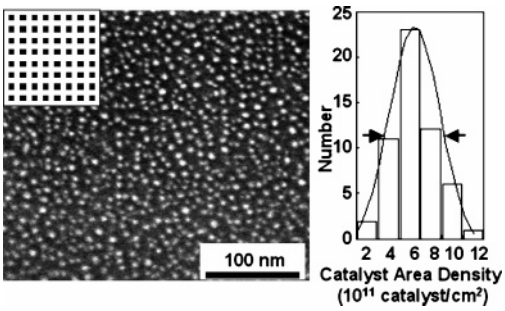

Figure 4. Catalyst area density. Typical SEM image of the Fe nanoparticles. Inset: Schematic illustration of the array pattern for the 64 SEM observations throughout the 2 × 2 cm^2 sample. Histogram: Catalyst area density histogram for all 64 observations fitted with a Gaussian distribution.

indistinguishable by SEM if in close proximity to a larger particle. However, from TEM observation of the tube diameter distribution, an insignificant fraction of the tubes are in the ~1 nm size range, and because it is well-accepted that the CNT diameter correlates to the catalyst size, we conclude that the number of missed small catalyst particles is quite negligible. Note: Due to the high density of particles, atomic force microscopy was found to be unsuccessful due to its limited lateral resolution. The density of catalyst nanoparticles was very uniform on a microscopic scale as shown in Figure 4, however, they also varied from point to point on a macroscopic scale. To account for this variance, 17 200 catalysts were counted from 64 distinct locations in an array pattern evenly spanning the entire 2×2 cm^2 substrate (Figure 4, inset). The calculated catalyst area density for each point was plotted as a histogram and fitted with a Gaussian curve from which we determined the mean value and SD (Figure 4, histogram). The average area density of catalysts was $6.2 \times 10^{11}(\pm 0.26 \times 10^{11})$ catalysts/cm^2[13] and from eq 1 the catalyst activity of super-growth was calculated to be $84 \pm 6\%$, which is an extremely high value when compared to the few percent activity in normal CVD, highlighting the effect of water acting as a catalyst activity enhancer. The immediate benefits of high catalyst activity extend beyond mass production of SWNTs, but more importantly the SWNT material would contain much less inactivated catalytic impurities thus enabling the immediate use of as-grown material without any purification. We would like to emphasize that the analysis of catalyst activity of 84% was implemented on an arbitrary sample, and no growth optimization had been carried out to maximize the catalyst activity. Therefore, we are confident that further improvements are possible by additional tuning of the super-growth to achieve catalyst activities close to 100%, one of the ultimate goals of SWNT synthesis. If 100% catalyst activity is achieved, significant breakthroughs could be realized in various fields, e.g., it might provide a solution for reliable assembly of CNT field effect transistors, opening up an exciting opportunity to realize integrated carbon nanotubes circuits. Considering the high catalyst activity of 84%, we envision that the emergence of super-growth CVD represents the end of the era where low catalyst activity had been one of the serious issues in SWNT synthesis.

In conclusion, we have developed a statistical and macroscopic approach to analyze SWNT forests and the catalyst activity of super-growth. Estimated values for a sample with typical catalysts and growth conditions are summarized in Table 1. Catalyst activity of super-growth is much higher than any reported growth clearly demonstrating the effect of water acting as a catalyst activity enhancer. We envision that even growth with catalyst activity close to 100% might be possible. The SWNT forest was found to be a very sparse material where SWNTs occupy only 3.6% of the total volume. This structural sparseness of the SWNT forest is believed to play a critical role in achieving highly efficient growth.

Acknowledgment. We gratefully acknowledge the helpful contributions by M. Mizuno, A. Otsuka, K. Ozawa, and S. Yamada. Partial support by the New Energy and Industrial Technology Development Organization (NEDO) Nano-Carbon Technology project and the use of the AIST Nano-Processing Facility are acknowledged.

References and Notes

(1) Hata, K.; Futaba, D. N.; Mizuno, K.; Namai, T.; Yumura, M.; Iijima, S. *Science* **2004**, *306*, 1362.

(2) Murakami, Y.; Chiashi, S.; Miyauchi, Y.; Hu, M.; Ogura, M.; Okubo, T.; Maruyama, S. *Chem. Phys. Lett.* **2004**, *385*, 298.

(3) Murakami, Y.; Einarsson, E.; Edamura, T.; Maruyama, S. *Phys. Rev. Lett.* **2005**, *94*, 87402.

(4) Hinds, B. J.; Chopra, N.; Rantell, T.; Andrews, R.; Gavalas, V.; Bachas, L. G. *Science* **2004**, *303*, 62.

(5) Ishida, M.; Hongo, H.; Nihey, F.; Ochiai, Y. *Jpn. J. Appl. Phys.* **2004**, *43*, L1356.

(6) (a) Hongo, H.; Nihey, F.; Ichihashi, T.; Ochiai, Y.; Yudasaka, M.; Iijima, S. *Chem. Phys. Lett.* **2003**, *380*, 158. (b) Seidel, R.; Liebau, M.; Duesberg, G. S.; Kreupl, F.; Unger, E.; Graham, A. P.; Hoenlein, W.; Pompe, W. *Nano Lett.* **2003**, *3*, 965. (c) Zhang, R. Y.; Amlani, I.; Baker, J.; Tresek, J.; Tsui, R. K. *Nano Lett.* **2003**, *3*, 731.

(7) Futaba, D. N.; Hata, K.; Yamada, T.; Mizuno, K.; Yumura, M.; Iijima, S. *Phys. Rev. Lett.* **2005**, *95*, 56104.

(8) Uncertainty in the estimation for the SWNT forest mass density is based on standard error propagation in calculation of the average density, where the density for each individual sample is calculated from the SWNT forest mass and its physical dimensions.

(9) (a) Rao, A. M; et al. *Science* **1997**, *275*, 187. (b) Bandow, S.; Asaka, A.; Saito, Y.; Rao, A. M.; Grigorian, L.; Richter, E.; Eklund, P. C. *Phys. Rev. Lett.* **1998**, *80*, 3779.

(10) (a) Taylor, J. R. *An Introduction to Error Analysis*, 2nd ed., University Science Books: Sausalito, CA, 1997; Chapters 4 and 5. (b) Uncertainty in the SWNT diameter distribution was estimated by using standard error analysis of the 407 measurements of the diameter. The average uncertainty in an individual measurement, the standard deviation (SD), was found to be 0.7 nm. The reported error value is the standard error of the mean, which is a measure of the uncertainty in the mean value as defined by $SD/\sqrt{N}$, where N is the number of measurements.

(11) Jorio A.; Saito, R.; Hafner, J. H.; Lieber, C. M.; Hunter, M.; McClure, T.; Dresselhaus, G.; Dresselhaus, M. S. *Phys. Rev. Lett.* **2001**, *86*, 1118.

(12) Error in the linear mass density follows directly from the linear relationship with the diameter. Therefore, through error propagation, the fractional error of both the diameter and the linear mass density are identical.

(13) The error in the catalyst area density estimation was identical with the error estimation for the mean diameter. The histogram of the 64 separate measurements of the density by SEM observation was fitted by a Gaussian distribution to obtain a standard deviation (SD). The reported error value is the standard error of the mean, which is a measure of the uncertainty in the mean value as defined by $SD/\sqrt{N}$, where N is the number of measurements.